

**MEASUREMENT OF THE SPIN STRUCTURE FUNCTION
 $G_1^P(X, Q^2)$ WITH CLAS AT JEFFERSON LAB**

YELENA PROK

*University of Virginia, Physics Department
 382 McCormick Road
 Charlottesville VA 22901, USA
 E-mail: yprok@jlab.org*

FOR THE CLAS COLLABORATION

Inelastic scattering using polarized nucleon targets and polarized charged lepton beams allows the extraction of the structure functions g_1 and g_2 which provide information on the spin structure of the nucleon. A program designed to study such processes has been underway in Jefferson Lab since 1998. A polarized electron beam, solid polarized NH_3 and ND_3 targets and the CEBAF Large Acceptance Spectrometer (CLAS) in Hall B were used to collect the desired data. The measurements cover the resonance region with unprecedented detail and add significantly to the DIS data set at low to moderate Q^2 and moderate to high x . The measured electron asymmetries are analyzed to produce quantities of interest, such as the photon-nucleon asymmetry A_1^p , the spin structure function g_1^p and its first moment Γ_1 .

1. Spin structure function g_1

For several decades spin structure functions have been measured using polarized nucleon targets and polarized lepton beams. In particular, the photon-nucleon asymmetry $A_1^p(x, Q^2)$, the structure function $g_1^p(x, Q^2)$, and its first moment $\Gamma_1(Q^2)$ have been subjects of great interest. The photon-nucleon asymmetry $A_1^p(x, Q^2)$ reflects the valence spin structure of the proton. In lowest order in the quark parton model, A_1^p is given by the ratio of the spin-dependent to spin-independent quark distribution functions¹:

$$A_1 = \frac{\sum_i e_i^2 [q_i^\uparrow - q_i^\downarrow]}{\sum_i e_i^2 [q_i^\uparrow + q_i^\downarrow]} \quad (1)$$

Assuming that the nucleon obeys $\text{SU}(6)$ symmetry generates the prediction that $A_1^p = 5/9$. While the $\text{SU}(6)$ predictions are approximately valid at $x \sim 0.3$, the symmetry is strongly broken, which is particularly evident at large

x . Several non-perturbative mechanisms have been used to account for this observation by explicitly breaking SU(6) at the quark level, which results in different weighting of components of the wavefunction, and consequently different x dependences for the spin and flavor distributions. Mapping A_1^p as a function of x can help differentiate between the various models.

The spin structure function g_1 is important in understanding the quark and gluon spin components of the nucleon spin, and their relative contributions in different kinematic regions. At high Q^2 , g_1 provides information on how the nucleon spin is composed of the spin of its constituent quarks and gluons. At low Q^2 , hadronic degrees of freedom become more important and dominate the measurements. Besides its Q^2 -dependence, g_1 depends also on the fraction of momentum, x carried by the struck parton. The DGLAP equations² predict that g_1^p increases logarithmically with Q^2 at low x , and decreases with Q^2 at high x . The first moment $\Gamma_1(Q^2)$ is obtained by integrating g_1 over the full range of x : $\Gamma_1(Q^2) = \int_0^1 g_1(x, Q^2) dx$. From the deep inelastic scattering experiments, the value of $\Gamma_1(Q^2)$ at high Q^2 is known to be positive and slowly varying. As Q^2 decreases, the nucleon resonances become important, and they cause $\Gamma_1(Q^2)$ to decrease rapidly. At $Q^2 = 0$, $\Gamma_1(Q^2)$ is bounded by the Gerasimov-Drell-Hearn sum rule^{4,3}, which relates the spin-dependent photo-nucleon cross sections to the anomalous magnetic moment κ of the target nucleon. Assuming a smooth connection between the real and virtual photo-nucleon cross sections, the GDH sum rule is generalized for the case of virtual photon scattering, which results in a prediction for the Q^2 -evolution of $\Gamma_1(Q^2)$ at low Q^2 . According to the GDH sum rule, $\Gamma_1^p(Q^2)$ approaches zero with a negative slope, and since $\Gamma_1^p(Q^2)$ is positive at high Q^2 , it must change sign at some low Q^2 . The low Q^2 region is dominated by nucleon resonances, and contains a transition from the hadronic to partonic degrees of freedom. This region remained largely unexplored until the recent experiments at Jefferson Lab.

2. Measurements and Analysis

A_1 and g_1 can be extracted from measurements of the double spin asymmetry $A_{||}$ in inclusive ep scattering:

$$\begin{aligned} A_1 &= A_{||}/D - \eta A_2 \\ g_1 &= \frac{F_1}{1 + \gamma^2} [A_{||}/D + (\gamma - \eta) A_2], \end{aligned} \quad (2)$$

where F_1 is the unpolarized structure function, A_2 is the virtual photon asymmetry, and γ , D and η are kinematic factors. F_1 and A_2 are calculated

using a parametrization of the world data, and A_{\parallel} is measured. The spin asymmetry for ep scattering is given by:

$$A_{\parallel} = \frac{N_- - N_+}{N_- + N_+} \frac{C_N}{fP_bP_t f_{RC}} + A_{RC}, \quad (3)$$

where $N_-(N_+)$ is the number of scattered electrons normalized to the incident charge with negative (positive) beam helicity, f is the dilution factor needed to correct for the electrons scattering off the unpolarized background, f_{RC} and A_{RC} correct for radiative effects, and C_N is the correction factor associated with polarized ^{15}N nuclei in the target. A_{\parallel} was measured by scattering polarized electrons off polarized nucleons using a cryogenic solid polarized target and CLAS in Hall B.

The longitudinally polarized electrons were produced by a strained *GaAs* electron source with a typical beam polarization of $\sim 70\%$. The solid polarized target consisted of ammonia beads placed in a 5 T magnetic field and cooled down to ~ 1 K by a liquid helium evaporation refrigerator. The target material had a high concentration of polarizable nucleons, and also contained paramagnetic centers which provided unpaired electron spins. The unpaired electrons were highly polarized in the 5 T magnetic field, and their polarization was transferred to the nucleons using microwaves to drive the hyperfine transitions between the polarized electrons and polarized nucleons. The target material used was ND_3 for polarized deuterons and NH_3 for polarized protons. The typical polarization was 70 – 90% for protons in the NH_3 target, and 10 – 35% for deuterons in the ND_3 target. Besides the polarized targets, three unpolarized targets were used for background measurements. These targets were solid ^{12}C , frozen ^{15}N , and an empty target filled with liquid ^4He . The scattered electrons were identified using the CLAS package, consisting of drift chambers, Cherenkov detector, time-of-flight counters and electromagnetic calorimeters. Data were taken with beam energies of 1.6, 2.4, 4.2 and 5.7 GeV, accumulating over 23 billion triggers. After the electron samples were selected, raw asymmetries were formed and corrected for various backgrounds. The unpolarized background consisted mostly of ^{15}N in the ammonia target, and we obtained its contribution by using the scattering data on ^{12}C target, and correcting it, taking into account differences between ^{12}C and ^{15}N . The method to determine P_bP_t was based on the knowledge of the theoretical value of the asymmetry for elastic ep scattering at given kinematics. Results from the inclusive and exclusive measurements were found to be consistent within the statistical errors, with the average value of $P_bP_t \sim 0.5$ for the

NH₃ target. The resulting asymmetries were also corrected for electrons from pair-symmetric processes, and for hadrons misidentified as electrons. Polarization-dependent internal radiative cross sections were calculated using the code developed by Kuchto and Shumeiko⁵. The external corrections were based on the work of Tsai⁶. To allow for the consistent propagation of errors, the radiative corrections are broken into an additive correction A_{RC} and a radiative dilution factor f_{RC} .

3. Results

Preliminary results for A_1^p are shown in Figure 1. Along with the EG1b data, the plot shows results from previous experiments, and predictions from several models. The models⁷ include the suppression of transitions to states in the lowest even and odd parity multiplets with combined quark spin $S = 3/2$, the suppression of transitions to states with helicity $h = 3/2$, and the suppression of transitions to states which couple only through symmetric components of the spin-flavor wavefunction. Also shown is the prediction of the hyperfine-perturbed quark model, which involves spin-spin interaction between the quarks, mediated by the one-gluon or pion exchange⁸. The values of

$A_1^p(x)$ extracted from the EG1b data show a preference for the pQCD limit as $x \rightarrow 1$, and are also consistent with the hyperfine-perturbed quark model. The left plot in Figure 2 shows preliminary results for g_1^p plotted as a function of x in bins of Q^2 . A strong resonant structure is evident at low Q^2 , with the $\Delta(1232)$ being the most prominent resonance, while the resonances become 'smoothed out' with growing Q^2 . This structure makes the first moment highly Q^2 -dependent at low Q^2 , as shown in the right-hand

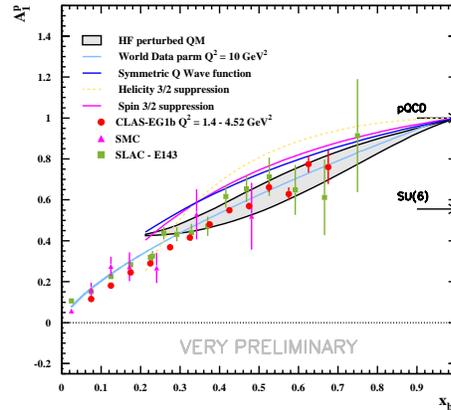


Figure 1. Asymmetry A_1^p plotted vs x could differentiate between the different models of valence spin structure of the proton. Two main predictions are indicated on the plot: pQCD: $A_1^p(x \rightarrow 1) \rightarrow 1$ and SU(6): $A_1^p = 5/9$.

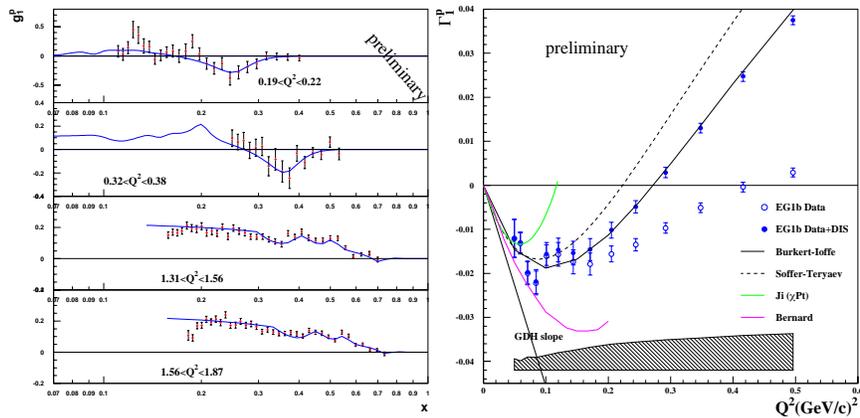


Figure 2. Left: Structure function g_1^p plotted vs x . Strong resonant structure is observed at low Q^2 . Right: Γ_1^p obtained with the 1.6 GeV data. Points shown by open circles are values of g_1^p integrated over the data down to the lowest available value of x . The missing part of the integral in DIS is obtained by integrating the 'Model' g_1^p down to $x = 0.001$. The two parts are added, and the sum is shown by filled circles. Systematic error is shown by a grey band on the bottom of the plot.

plot of Figure 2. Two different parametrization models^{9,10} are shown on the plot, along with the chiral perturbation predictions, and the GDH slope. We find that our data follow closely the Burkert-Ioffe parametrization¹⁰, and are consistent with two chiral perturbation models up to $Q^2 \approx 0.06$ GeV².

References

1. P. Renton, *Electroweak Interactions*, (Cambridge University Press) (1990).
2. G. Altarelli and G. Parisi, *Nucl. Phys.* **B126**, 298 (1977).
3. S. Drell and A. Hearn, *Phys. Rev. Lett.* **16**, 908 (1966).
4. S. Gerasimov, *Yad. Fiz.* **2**, 598 (1965).
5. T. V. Kuchto and N. M. Shumeiko, *Nucl. Phys.* **B219**, 412-436 (1983).
6. L. W. Mo and Y. S. Tsai, *Rev. Mod. Phys.* **41**, 1 (1969).
7. F. E. Close and W. Melnitchouk, *hep-ph/0302013* (2003).
8. N. Isgur, *Phys. Rev. D* **59**, 034013 (1999).
9. J. Soffer and O. Teryaev, *Phys. Rev. D* **51**, 25 (1992).
10. V. Burkert and B. Ioffe, *Phys. Lett. B* **296**, 223 (1992).